ResearchGate

See discussions, stats, and author profiles for this publication at: https://www.researchgate.net/publication/281607940

A Detailed Study on Phosphor-Converted Light-Emitting Diodes With Multi-Phosphor Configuration Using the...

Article *in* IEEE Journal of Quantum Electronics · October 2015

DOI: 10.1109/JQE.2015.2472341

CITATIONS
12

READS
103

7 authors, including:

Jia-Sheng Li
South China University of Technology
10 PUBLICATIONS **30** CITATIONS

SEE PROFILE

Zongtao Li
South China University of Technology
51 PUBLICATIONS **381** CITATIONS

SEE PROFILE

Xinrui Ding
University of California, Berkeley
26 PUBLICATIONS **124** CITATIONS

SEE PROFILE

Some of the authors of this publication are also working on these related projects:

Project
Quantum dots synthesis and application View project

Project
photoelectric characteristics of Silicon single-nanowire and its application in solar cells View project

All content following this page was uploaded by Xinrui Ding on 03 November 2015.

The user has requested enhancement of the downloaded file.

A Detailed Study on Phosphor-Converted Light-Emitting Diodes With Multi-Phosphor Configuration Using the Finite-Difference Time-Domain and Ray-Tracing Methods

Jia-Sheng Li, Jia-Xiao Chen, Li-Wei Lin, Zong-Tao Li, Yong Tang, Bin-Hai Yu, and Xin-Rui Ding

***Abstract*— Although the optical simulations have been widely adopted to study phosphor-converted light-emitting diodes (pcLEDs), to the best of our knowledge, there is no study that investigates the pcLED model considering the effect of phosphor particles with irregular shapes. In order to explore this topic, we employ the finite-difference time-domain method to characterize the phosphor-converted element (PCE) model. Furthermore, the PCE-based pcLED with YAG:Ce and nitride phosphors is investigated by the ray-tracing method. The results show that the rod-shaped nitride phosphor can scatter incident light to larger angles compared with the spherical YAG:Ce phosphor of the same size. In turn, their different scattering and absorption characterizations cause that the mixing concentration of the phosphors has a significant effect on the correlative color temperature and light output power of the pcLED.**

***Index Terms*— Optical simulation, light-emitting diodes (LEDs), finite-difference time-domain (FDTD), multi-phosphor configuration.**

I. Introduction

LIGHT-EMITTING diodes (LEDs) are considered to hold significant potential in next-generation solid-state lighting (SSL) applications on account of their many advantages [1]. One of the most promising methods to generate white light is by combining a blue LED chip with phosphor-converted elements (PCEs); LEDs that adopt this method are referred to as phosphor-converted LEDs (pcLEDs). The PCE configuration critically affects the optical performance of pcLEDs, in particular their angular color uniformity (ACU), light output efficiency (LE), etc. Consequently, many people have studied the effect of PCEs on pcLEDs numerically, and in terms of the particles size [2]–[4], the extinction coefficient [5], the concentration [6]–10], the distance from source [11], and the geometric morphology [12]–[16].

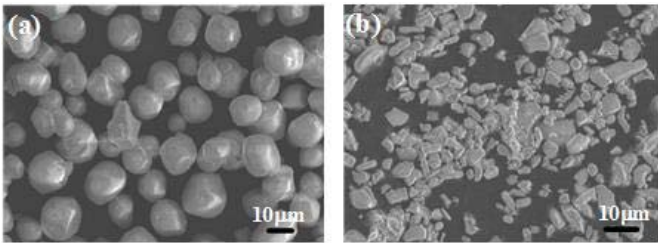

Fig. 1. Scanning electron microscope (SEM) images of (a) YAG:Ce phosphors and (b) nitride phosphors.

Most of these studies simply focus on the YAG phosphor because of its excellent luminescent characteristics, long lifetime, and impressive stability [17], [18]. However, using the single YAG phosphor configuration, it is hard to achieve a high color rendering index (CRI) and a low correlative color temperature (CCT) [19], thereby making it increasingly difficult to satisfy the increasing demand for pcLEDs. In order to expand the excitation spectrum of the PCE and obtain a high CRI, a common approach proceeds by combining nitride phosphors with YAG phosphors [20]. Some studies on this multi-phosphor configuration have also been carried out experimentally [21]–[24]. However, to the best of our knowledge, the pcLED with multi-phosphor configuration has barely been studied through optical simulations, unlike the single YAG phosphor configuration. This is mainly because of the fact that the present studies tend to employ the Monte Carlo method [25] in order to simulate light propagation in the PCE, which is regarded as YAG phosphors particles cloud mixed with silicone. In turn, the optical properties of the PCE are solved via the Mie scattering model [26]. As far as we know, the Mie scattering model is the only exact mathematical solution of scattering parameters for the homogeneous spherical particles. As a result, the PCE model is more suitable for spherical phosphor particles, such as the nearly spherical YAG phosphor shown in Fig. 1(a).

However, the nitride phosphor, which is broadly used in the multi-phosphor configuration, has a mostly non-spherical

Manuscript received June 3, 2015; revised August 17, 2015; accepted August 20, 2015. Date of publication August 24, 2015; date of current version September 4, 2015. This work was supported in part by the Post-Doctoral Science Foundation of China under Grant 2014M560659 and in part by the National Natural Science Foundation of China under Grant 51375177, Grant 51405161, and Grant U1401249. *(Corresponding author: Z.-T. Li.)*

J.-S. Li, J.-X. Chen, Y. Tang, B.-H. Yu, and X.-R. Ding are with the Key Laboratory of Surface Functional Structure Manufacturing of Guangdong, Higher Education Institutes, South China University of Technology, Guangzhou 510641, China.

L.-W. Lin is with the Department of Mechanical Engineering, University of California at Berkeley, Berkeley, CA 94720-5800 USA.

Z.-T. Li is with the Key Laboratory of Surface Functional Structure Manufacturing, Guangdong, Higher Education Institutes, South China University of Technology, Guangzhou 510641, China, and also with Foshan Nationstar Optoelectronics Company, Ltd., Foshan 528000, China (e-mail: meztli@scut.edu.cn).

Color versions of one or more of the figures in this paper are available online at http://ieeexplore.ieee.org.

Digital Object Identifier 10.1109/JQE.2015.2472341

0018-9197 © 2015 IEEE. Personal use is permitted, but republication/redistribution requires IEEE permission.
See http://www.ieee.org/publications_standards/publications/rights/index.html for more information.

shape, as shown in Fig. 1(b). It is known that the Mie results lead to significant discrepancies for non-spherical particles in the scattering phase function (SPF), especially at the large forward scattering angles and at backward scattering angles [27], [28]. If we still adopt the Mie scattering model to characterize a PCE including irregularly shaped nitride phosphors, the simulated results of the multi-phosphor configuration may cause some non-negligible errors.

Certain methods exist for dealing with the PCE model for pcLEDs that are not limited to the actual shapes of phosphor particles. For instance, Hsiao *et al*. developed a PCE model using the measured near-field chromatic luminance data to define the effective phosphor particle radius that best describes the scattering effect of a real PCE [29]. Furthermore, Hung and Tien [30] and Chen *et al.* [31] have introduced the bidirectional scattering distribution function (BSDF) to describe the optical properties of the PCE, the BSDF data are obtained experimentally. Their simulated results exhibit impressive agreement with the experiments. However, once the PCE configuration changes – for instance, in terms of its phosphor particle size distribution, concentration, geometry, etc., – it is necessary to measure the chromatic luminance data or BSDF data again. This approach is therefore inconvenient for predicting the effect of the PCE on pcLEDs.

Contrastingly, the finite-difference time-domain (FDTD) method is not limited to particle shapes, and can obtain the optical properties of the PCE numerically. This method is widely adopted for analyzing the scattering properties of non-spherical particles [32], and furthermore displays impressive agreement with the Mie results for spherical particles [27]. However, despite our best efforts, we have not identified any studies that combine the FDTD method and the PCE model in pcLED simulations.

In what follows, we propose an effective methodology for defining the optical properties of PCEs in pcLEDs by employing the FDTD method. Finally, the CCT and light output power P_{opt} of the pcLED with a multi-phosphor configuration are investigated.

II. The PCE Characterization

A. The Scattering and Absorption Parameters of Phosphor Particles

The FDTD method is employed to define the scattering cross-section C_{sca}, the absorption cross-section C_{abs}, and the SPF of phosphor particles. In the FDTD calculation region, the electromagnetic fields are solved on discrete time and space intervals according to the Maxwell's equations. In the scattering parameters calculation, the FDTD calculation region is divided into the scattered field region and the total field region. In the total field region, the incident source electromagnetic field and the scattered electromagnetic field are included in the calculation; on the other hand, in the scattered field region, only the scattered electromagnetic field is calculated. Therefore, the total scattered power $P_{\mathrm{sca}}(\lambda)$ and the total power absorbed by the particles $P_{\mathrm{abs}}(\lambda)$ can be calculated according to the following equations:

$$P_{\mathrm{sca}}(\lambda) = \sum_{i=1}^{n} T_{\mathrm{i}}^{\mathrm{scattered}}(\lambda)\, P_{\mathrm{source}}(\lambda), \tag{1}$$

$$P_{\mathrm{abs}}(\lambda) = (1 - \sum_{i=1}^{n} T_{\mathrm{i}}^{\mathrm{total}}(\lambda)) P_{\mathrm{source}}(\lambda), \tag{2}$$

where $T_{\mathrm{i}}^{\mathrm{scattered}}(\lambda)$ and $T_{\mathrm{i}}^{\mathrm{total}}(\lambda)$ are the scattered transmission and total transmission obtained from a series of monitor surfaces in the scattered field region and the total field region, respectively; $P_{\mathrm{source}}(\lambda)$ is the incident source power (W); λ is the wavelength (nm).

Next, the C_{sca} and the C_{abs} can be calculated according to the following equations [33]:

$$C_{\mathrm{sca}}(\lambda) = \frac{P_{\mathrm{sca}}(\lambda)}{I_{\mathrm{source}}(\lambda)}, \tag{3}$$

$$C_{\mathrm{abs}}(\lambda) = \frac{P_{\mathrm{abs}}(\lambda)}{I_{\mathrm{source}}(\lambda)}, \tag{4}$$

where $I_{\mathrm{source}}(\lambda)$ is the source irradiance (W/m^2).

Besides the cross-section properties, the SPF $p(\lambda, \theta, \phi)$ is also an important scattering parameter for describing the normalized scattering energy distribution in the far field. It is defined as follows [34]:

$$p(\lambda, \theta, \phi) = \frac{4\pi F(\lambda, \theta, \phi)}{k_0^2 C_{\mathrm{sca}}(\lambda)}, \tag{5}$$

where $F(\lambda, \theta, \phi)$ is the dimensionless scattering function, k_0 is the wavenumber (m^{-1}), and θ and ϕ are the zenith and azimuth angles. Because the SPF is satisfied by the normalization condition [35], it can be also written in a simplified form, as follows:

$$p(\lambda, \theta, \phi) = \frac{P_{\mathrm{sca}}^{\mathrm{far}}(\lambda, \theta, \phi)}{P_{\mathrm{sca}}(\lambda)}, \tag{6}$$

where $P_{\mathrm{sca}}^{\mathrm{far}}(\lambda, \theta, \phi)$ is far-field scattering power in a discrete region $\{(\theta_{\mathrm{s}},\ \phi_{\mathrm{s}}) \mid \theta + \Delta\theta > \theta_{\mathrm{s}} \geq \theta,\ \phi + \Delta\phi > \phi_{\mathrm{s}} \geq \phi\}$. In far-field spherical coordinates, $P_{\mathrm{sca}}^{\mathrm{far}}(\lambda, \theta, \phi)$ can be calculated as follows [36]:

$$P_{\mathrm{sca}}^{\mathrm{far}}(\lambda, \theta, \phi) = \int_{\phi}^{\phi+\Delta\phi} \int_{\theta}^{\theta+\Delta\theta} S(\lambda, \theta_{\mathrm{s}}, \phi_{\mathrm{s}}) R^2 \sin\theta_{\mathrm{s}} \mathrm{d}\theta_{\mathrm{s}} \mathrm{d}\phi_{\mathrm{s}}, \tag{7}$$

where $S(\lambda, \theta_{\mathrm{s}}, \phi_{\mathrm{s}})$ is the module of the Poynting vector (W/m^2), R is the distance from the observation point to the particle (m).

B. The Optical Properties of the PCE

To combine the scattering and absorption characterization of YAG and nitride phosphors with the pcLED model, the Monte Carlo ray-tracing method is widely applied. When studying light propagation through a PCE consisting of particle clouds, there are three parameters used in the Monte Carlo light scattering model [25]: the absorption coefficient μ_{abs}, the scattering coefficient μ_{sca}, and the scattering phase function p_{PCE}. It is assumed that there are negligible particle interaction effects and multiple scattering events inside particle clouds

at a low particle concentration. Therefore, the $P_{\text{sca}}(\lambda)$ and the $P_{\text{abs}}(\lambda)$ of every phosphor particle can be added directly to obtain the total scattering and absorption power of the PCE [33]. With the equations (3) to (6), the three parameters of the PCE including one type of phosphor with different particle size take on the following forms:

$$\mu_{\text{abs,i}}(\lambda) = N_{\text{i}} \frac{\bar{P}_{\text{abs,i}}(\lambda)}{I_{\text{source}}(\lambda)} = \frac{c_{\text{i}}}{\bar{m}_{\text{i}}} \bar{C}_{\text{abs,i}}(\lambda), \tag{8}$$

$$\mu_{\text{sca,i}}(\lambda) = N_{\text{i}} \frac{\bar{P}_{\text{sca,i}}(\lambda)}{I_{\text{source}}(\lambda)} = \frac{c_{\text{i}}}{\bar{m}_{\text{i}}} \bar{C}_{\text{sca,i}}(\lambda), \tag{9}$$

$$p_{\text{CCE,i}}(\lambda, \theta, \phi) = \frac{\int p_{\text{i,D}}(\lambda, \theta, \phi)\, C_{\text{sca,i,D}}(\lambda)\, n_{\text{i}}(D) dD}{\int C_{\text{sca,i,D}}(\lambda)\, n_{\text{i}}(D) dD}, \tag{10}$$

where N_i is the total number of type i phosphor particles per unit volume (1/m^3), $\bar{P}_{\text{abs,i}}(\lambda)$ and $\bar{P}_{\text{sca,i}}(\lambda)$ is the average absorption and scattering power of the type i phosphor with different particle size D respectively, c_i is the type i phosphor particle concentration (g/m^3), $n_{\text{i}}(D)$ is the type i phosphor particle size distribution function, $p_{\text{i,D}}(\lambda, \theta, \phi)$ and $C_{\text{sca,i,D}}$ is the scattering phase function and the scattering cross-section of the type i phosphor with particle size D respectively; $\bar{C}_{\text{abs,i}}(\lambda)$, $\bar{C}_{\text{sca,i}}(\lambda)$, and $\bar{m}_{\text{i}}$ are the absorption, scattering cross-section, and the particle mass of the type i phosphor integrated over $n_{\text{i}}(D)$, respectively. These quantities, in turn, can be calculated with the following equations:

$$\bar{C}_{\text{abs,i}}(\lambda) = \frac{\int C_{\text{abs,i,D}}(\lambda)\, n_{\text{i}}(D) dD}{\int n_{\text{i}}(D) dD}, \tag{11}$$

$$\bar{C}_{\text{sca,i}}(\lambda) = \frac{\int C_{\text{sca,i,D}}(\lambda)\, n_{\text{i}}(D) dD}{\int n_{\text{i}}(D) dD}, \tag{12}$$

$$\bar{m}_{\text{i}} = \frac{\int m_{\text{i}}(D)\, n_{\text{i}}(D)\, dD}{\int n_{\text{i}}(D) dD}, \tag{13}$$

where $C_{\text{abs,i,D}}(\lambda)$ and $m_{\text{i}}(D)$ is the absorption cross-section and particle mass of the type i phosphor with particle size D.

Based on the same assumption above, the parameters of the PCE with k types of phosphor can be calculated as follows:

$$\mu_{\text{abs}}(\lambda) = \sum_{i=1}^{k} \mu_{\text{abs,i}}(\lambda), \tag{14}$$

$$\mu_{\text{sca}}(\lambda) = \sum_{i=1}^{k} \mu_{\text{sca,i}}(\lambda), \tag{15}$$

$$p_{\text{CCE}}(\lambda, \theta, \phi) = \frac{\sum_{i=1}^{k} N_{\text{i}} \bar{C}_{\text{sca,i}}(\lambda)\, p_{\text{CCE,i}}(\lambda, \theta, \phi)}{\iint \sum_{i=1}^{k} N_{\text{i}} \bar{C}_{\text{sca,i}}(\lambda)\, p_{\text{CCE,i}}(\lambda, \theta, \phi) d\theta d\phi}. \tag{16}$$

III. Experiment and Simulation Setup

The common YAG:Ce and nitride phosphors that were adopted in our previous study [23] are further investigated in this paper. The density and refractive index of the YAG:Ce phosphors are 4.5 g/cm^3 and 1.78, respectively; for the nitride phosphors, these quantities are 4.5 g/cm^3 and 2.17, respectively. In order to define the particles sizes and simplified shapes, we measured the particles size distributions with scanning electron microscopy (SEM), as shown above in Fig. 1. From these images, we can see that the YAG:Ce phosphor particles are nearly spherical, whereas the nitride phosphor particles are nearly rod shaped. Therefore, the YAG:Ce phosphor is assumed to be spherical, which is the same with most of the studies on pcLEDs simulation, whereas the other phosphor is assumed to be rod shaped, with different lengths and widths. In addition, the particles size distributions and some typical shapes are shown in Fig. 2. We regard the YAG:Ce and nitride phosphor particle sizes as the diameter and the diagonal covering the entire phosphor particle, respectively. On the basis of these SEM measurements, the YAG:Ce phosphor and nitride phosphor have an average particle size of 13.7 μm and 5.2 μm, respectively, and a standard deviation of 5.0 μm and 4.0 μm, respectively.

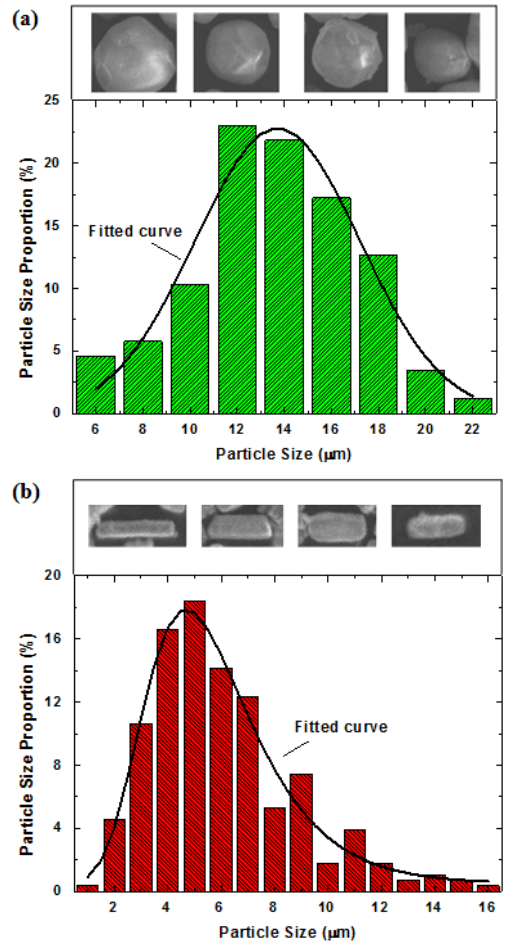

Fig. 2. The particle size distributions for (a) YAG:Ce and (b) nitride phosphors.

In the simulation, the commercial software packages FDTD Solutions and Tracepro were used. Fig. 3(a) shows the detailed modeling of YAG:Ce phosphors by the FDTD method. The simplified model (SM) of the YAG:Ce phosphor was placed in a three-dimensional FDTD simulation region (3D simulation mode), which was truncated by the perfectly matched layer (PML). In order to divide the simulation region into the total filed region and the scattered field region, the total-field scattered-field source (TS-source) with a center wavelength

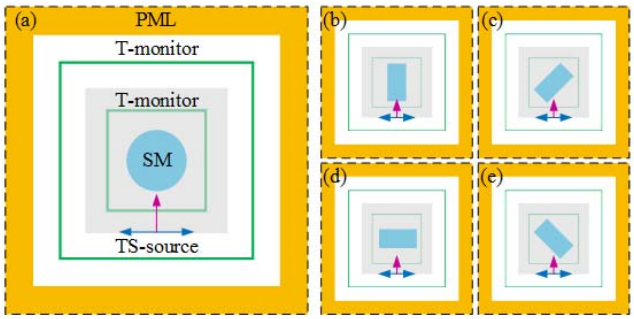

Fig. 3. The detailed finite-difference time-domain (FDTD) model for (a) YAG:Ce and (b)–(e) nitride phosphors. PML: Perfectly matched layer. TS-source: total-field scattered-field source. T-monitor: transmission-monitor. SM: simplified model.

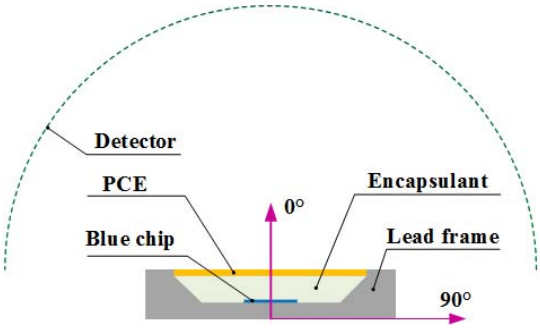

Fig. 4. The ray-tracing model of the phosphor-converted light-emitting diode (pcLED). PCE: phosphor-converted element.

of 455 nm was applied, which surrounded the SM of the YAG:Ce phosphor. The transmission-monitor (T-monitor) box consisted of a series of plane monitors, which were used for recording the electromagnetic field information passing through the monitors. The background index was depended on the medium surrounding the phosphor. Similarly, the detailed modeling of the nitride phosphor similar to that of the YAG:Ce phosphor, except for its SM and different angles of orientation. When setting up the optical model of the PCE, which consisted of particle clouds, it was necessary to assume that the phosphor particles were randomly oriented [33]. This means that the probability that the incident light propagates into the phosphor particles should be the same for each angle. Consequently, we defined the average cross-section and SPF of phosphor particles oriented at different angles in terms of the results obtained from phosphor particles that were oriented randomly.

As for the YAG:Ce phosphor particle, which was simplified as being spherical, it was easily to account for the random orientation given its symmetry. However, for the nitride phosphor, it was necessary to consider a variety of angles in order to obtain properly random results. Therefore, we placed the SM of the nitride phosphor at 0°, 45°, 90°, and 135°, and considered the simulation efficiency and accuracy [see Figs. 3(b)–(e)]. It should be noted that the subsequent discussion on the cross-section and SPF is based on the randomly oriented phosphor particles.

The ray-tracing modeling is shown in Fig. 4. The commercially available pcLED was composed of a blue LED chip with a Lambertian distribution, a commercial plastic lead frame package with 90% reflectance, the encapsulant, and a PCE. The encapsulant was made from silicone; its index of refraction was 1.54, and it was assumed that the silicone was no absorption for light. The PCE contained the YAG:Ce phosphors, nitride phosphors, and silicone; its conversion efficiency was 75%, and its index of refraction depended on the concentrations of these two types of phosphors. The emission spectra of the blue LED chip was centered at 455 nm, whereas that of the PCE was centered at 525 nm and 620 nm (because of the mixing of the YAG:Ce and nitride phosphors) [23]. (The detailed properties of the PCE will be discussed in next section.) In order to record the far-field CCT distribution and P_{opt}, a semi-spherical detector with a 1 m radius was placed upon the pcLED.

IV. Results and Discussion

A. The Scattering and Absorption Characterizations of Phosphor Particles

Firstly, we consider the 8 μm YAG:Ce and nitride phosphors as an example in order to discuss their scattering characterization through the electromagnetic field distribution, which is shown in Fig. 5. It can be observed from Fig. 5(a) that the light wave takes on a fan shape that consists of a series of continuously curved waves that gather toward the top region of the phosphor. After being scattered by the YAG:Ce phosphor, the propagation of the light wave is still regular, and most of the light wave is emitted from the top surface. Nevertheless, from Figs. 5(b)–(e) we can see that the propagation of the light wave in the nitride phosphor is quite different. It is difficult to discern an obvious propagation direction inside the nitride phosphor, it seems that the incident light wave is broken into many fragments by the scattering effect. However, the light wave inside the nitride phosphor is more uniform, and does not gather toward the top region, as does the YAG:Ce phosphor. Also, the light wave that is emitted from the surface is more uniform, though the light wave inside the phosphor is quite irregular.

We believe that these differences are mainly caused by the effect of the morphology of the phosphor particles on the incident light wave. To achieve a deeper understanding of this effect, we further discuss nitride phosphor particles that are oriented at different angles. When the nitride phosphor particle is oriented at 0° (Fig. 5(b)), a large number of light waves are reflected backward, and only a slight amount of light is scattered forward from the upper surface. However, when oriented at 45° (Fig. 5(c)), more light is uniformly scattered from the left surface, and its emission direction seems to be deflected an angle compared to its incident direction. As for being oriented at 90° (Fig. 5(d)), more light is scattered forward from the upper surface as compared with the 0° orientation because the entrance for the incident light wave that propagates into the phosphor becomes larger. When light propagates perpendicularly into the surface of the nitride phosphor, we find that the emission direction is generally the same as the incident direction. Otherwise, the emission direction can generally be deflected an angle.

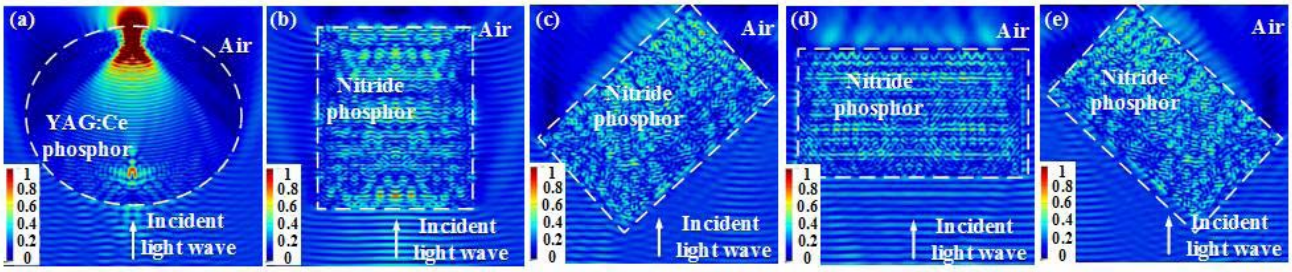

Fig. 5. The cross-sectional view of the electromagnetic field distribution for 8 μm (a) YAG:Ce phosphor particle and (b)–(e) nitride phosphor particles oriented at 0°, 45°, 90° and 135° respectively.

As for the spherical YAG:Ce phosphor, its lower surface can be divided into many sub-surfaces, and the incident angles for every sub-surface will be different. As a result, the deflected angles are also different at every sub-surface, which may lead to the gathering of the light wave in the top region of YAG:Ce phosphor.

To have a better understanding of the scattering ability for the randomly oriented YAG:Ce and nitride phosphors, we further discuss their far-field scattering power distributions at three typical particles sizes: 1 μm, 8 μm, and 16μm. Fig. 6 shows their scattering phase distributions (SPDs). Three critical incident wavelengths of blue light (455 nm), yellow-green light (525 nm), and red light (620 nm) are considered. At small particles sizes, the SPDs of the YAG:Ce phosphor and nitride phosphor are slightly sensitive to the incident wavelength; in particular, the longer wavelength can lead to a slightly stronger scattering effect, which can be seen in Figs. 6(a) and (d); At larger particles sizes, the differences caused by these three wavelengths can be ignored because the changes of the wavelengths are quite smaller than the particle size (16 μm). But no matter for which wavelength, as the particles size increases, the scattering effect on the incident light of both phosphors becomes weaker. This is primarily reflected in the changes of the scattering phase at the 0° direction $p(0°)$. As the particle size increases, the $p(0°)$ becomes larger.

From Figs. 6(a) and (c) and Figs. 6(d) and (f) we can see that the $p(0°)$ for a particle size of 16 μm is two orders of magnitude larger than that for a particle size of 1 μm; this means that more incident light is not deflected and still propagates along the original incident direction (0° direction) for larger particles sizes. On the other hand, as the particles size increases, the scattering uniformity of both phosphors also decreases. As for the YAG:Ce and nitride phosphors with sizes of 1 μm and under an incident wavelength of 455 nm, the standard deviations of their SPDs p_{dev} are 1.75 and 0.86, respectively; whereas for the phosphors with sizes of 16 μm, the p_{dev} are 27.56 and 15.68, respectively. Therefore, the SPD is more uniform at smaller particle sizes. This demonstrates that the smaller phosphor particles have stronger abilities to scatter the incident light and obtain a more uniform SPD.

Comparing the nitride phosphor with the YAG:Ce phosphor, we see that the $p(0°)$ for the nitride phosphor is generally one order of magnitude smaller than that of YAG:Ce phosphor of the same size. Moreover, the SPD is also more uniform for the nitride phosphor. These two factors imply that that the scattering ability of the nitride phosphor is more outstanding. Based on the electromagnetic field distribution mentioned above, one reasonable explanation is that the rod-shaped nitride phosphor can scatter the incident light to a large angle when being oriented at different angles, which is also helpful in achieving a more uniform SPD. On the other hand, owing to the symmetry of the YAG:Ce phosphor, most of the incident light still emits along the incident direction, regardless of

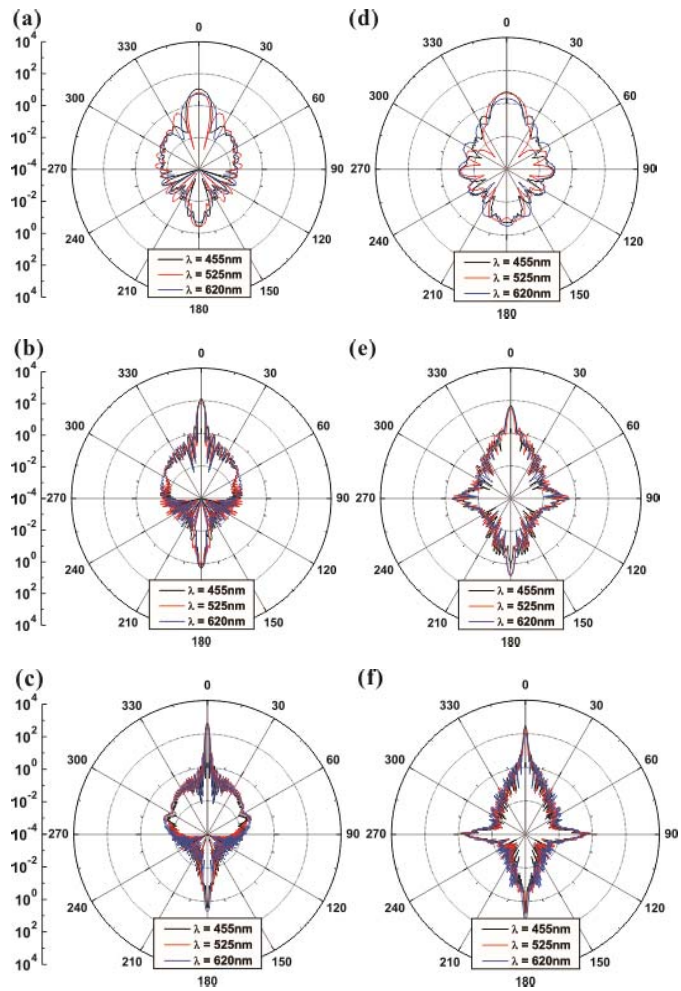

Fig. 6. The scattering phase distributions (SPDs) of (a)–(c) YAG:Ce phosphors and (d)–(f) nitride phosphors with particle sizes of 1 μm, 8 μm, and 16 μm, respectively.

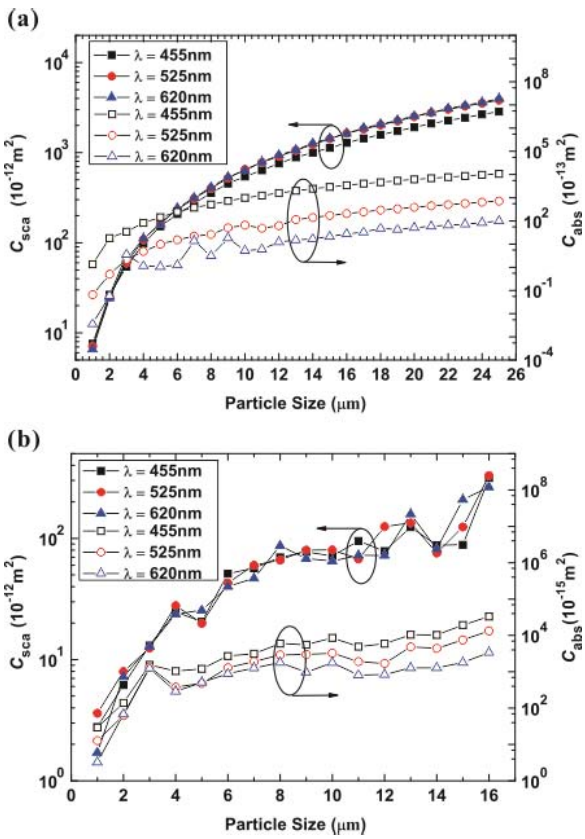

Fig. 7. The scattering cross-section C_{sca} and absorption cross-section C_{abs} of (a) the YAG:Ce phosphor and (b) the nitride phosphor.

how the phosphors are oriented. It can be inferred that if the nitride phosphor is also assumed to be spherical or solved by the Mie method, its scattering ability may become much weaker. Moreover, we can also see that the nitride phosphor has a larger backward scattering power because of its higher refractive index.

Fig. 7 shows the C_{sca} and C_{abs} of the YAG:Ce phosphor and the nitride phosphor. We find that their C_{sca} and C_{abs} values increase as the particle size increases for blue light (455 nm), yellow-green light (525 nm), and red light (620 nm). This means that much more incident power turns into scattering power and absorption power. This is mainly the result of the fact that the scattering and absorption properties of particles primarily depend on the projected area in the case that the particle size is larger than the wavelength [28]. Obviously, with the increasing particle size (i.e., the diameter of the spherical particles and the diagonal of the rod-shaped particles), the projected area of the phosphor particles increases as the square of that size, while the increasing tendency of the cross-section values becomes slower. In other words, the scattering and absorption cross-section of the phosphor particles is more sensitive for smaller particle sizes.

By comparing their cross-sections, it can be seen that the cross-section of the YAG:Ce phosphor is generally one order of magnitude larger than that of the nitride phosphor of the same size. This means that the YAG:Ce phosphor has a higher scattering power and absorption power. One reasonable explanation is that the projected area of the spherical YAG:Ce phosphor is π times of that of the rod-shaped nitride phosphor. Furthermore, the C_{sca} is at least one order of magnitude larger than the C_{abs} of both phosphors, which means that the phosphor particles can turn more incident power into scattering power in the light propagating process. Moreover, C_{sca} varies little across different wavelengths owing to the fact that the difference between these three wavelengths is much smaller than the particle size. However, C_{abs} is quite sensitive to the wavelength, which can be also seen from the absorption spectra of the YAG:Ce and nitride phosphors [23]. Both phosphors have a strong absorption effect on blue light (455 nm); moreover, the C_{abs} (455 nm) is nearly two orders of magnitude larger than C_{abs} (620 nm) for the same particle size.

B. The Optical Properties of the PCE

Based on the scattering and absorption characterizations of the YAG:Ce and nitride phosphors discussed above, the optical properties of the PCE with different YAG:Ce and nitride phosphor concentrations are given in Fig. 8. From Figs. 8(a)–(c), it can be seen that μ_{sca} and μ_{abs} increase with the increasing total phosphor concentration c_{Y+N}, which means that the probability of scattering and absorption also increases inside the PCE [25]. The reason for this is that as the total number of phosphors per unit volume becomes larger; thus the incident light is more easily scattered by the phosphors, which is similar to the results of studies on the single YAG phosphor configuration [34]. Similarly, μ_{sca} also increases as the nitride phosphor concentration c_N increases for a particular c_{Y+N}, which demonstrates that the nitride phosphor contributes much more strongly to the scattering ability of the PCE.

Two reasons for this observation can be provided. First, the nitride phosphor has a smaller density compared with the YAG:Ce phosphor, and its total volume is so large at a certain concentration that the incident light more easily propagates in it. As a result, the probability of scattering also increases. Second, the mean particles size of the nitride phosphor is much smaller, which leads to a stronger scattering ability. In other words, it has a higher probability of scattering per unit distance of light propagation. In fact, the total volume of the nitride phosphor is larger than that of the YAG:Ce phosphor within 5% at a certain concentration. Therefore, the second of the two points just mentioned seems to be the primary factor. The tendency of μ_{abs} for different concentrations is generally the same as μ_{sca} except for μ_{abs} (455 nm), which shows that the YAG:Ce phosphor still has stronger absorption ability per unit volume for blue light, thought it has a larger particle size.

In addition, the μ_{sca} for blue light (455 nm), yellow-green light (525 nm), and red light (620 nm) is almost the same, whereas the μ_{abs} differs greatly. In particular, μ_{abs} (455 nm) is generally one order of magnitude larger than μ_{abs} (525 nm) and μ_{abs} (620 nm). This demonstrates that the PCE emits the converted light mainly depended on the absorption for blue light, and the absorption for its converted light is much weaker. Therefore, though μ_{abs} (525 nm) and μ_{abs} (620 nm) increase as c_N increases for a particular c_{Y+N}, the influence of the decreasing μ_{abs} (455 nm) on the absorption properties

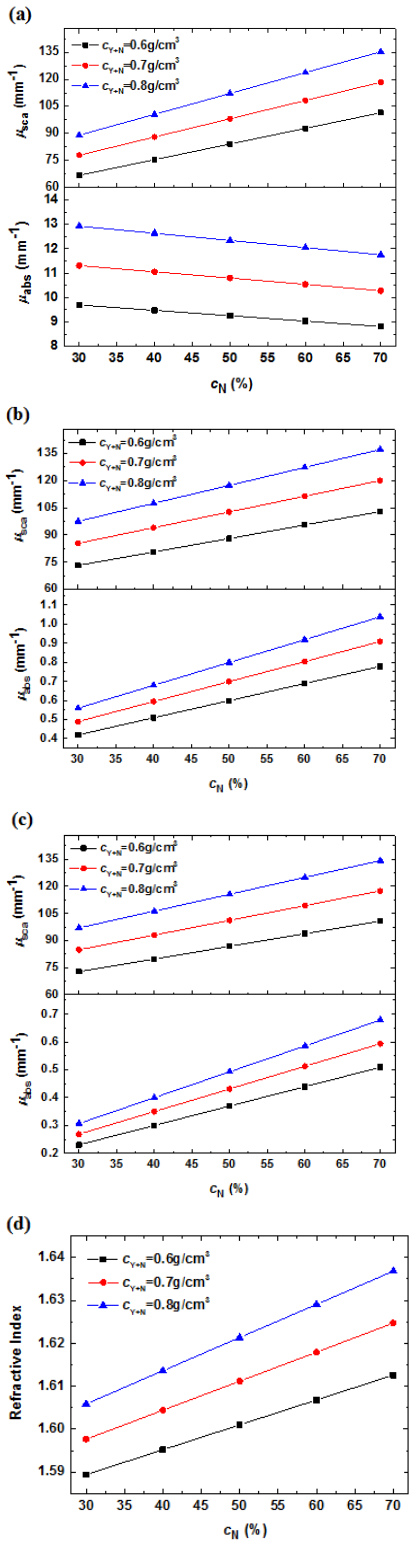

Fig. 8. The scattering and absorption coefficients, μ_{sca} and μ_{abs}, of the phosphor-converted element (PCE) under different nitride phosphor concentration c_N for (a) blue light (455 nm). (b) yellow-green light (520 nm), and (c) red light (620 nm). (d) The refractive index of the PCE.

of the PCE is much stronger, resulting in the total amount of converted light decreasing as c_N increases. Fig. 8(d) also shows that the increasing c_N can lead to a higher refractive index of the PCE, which causes a stronger total reflection effect.

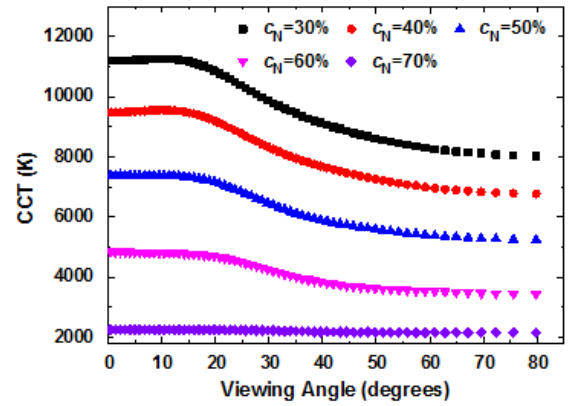

Fig. 9. The correlative color temperature (CCT) distribution of the phosphor-converted light-emitting diode (pcLED) with multi-phosphor configuration.

C. The Optical Performance of the pcLED

According to the optical properties of the PCE, the pcLED with multi-phosphor configuration is simulated by the ray-tracing method. Fig. 9 shows its CCT distribution with $c_{Y+N} = 0.6$ g/cm^3, from which it can be found that the CCT distribution is much higher in its central viewing angles. With the increasing c_N, the CCT generally decreases, and its distribution becomes more uniform. As discussed above, with more nitride phosphors, the PCE has stronger scattering ability and a higher refractive index. This means that the total propagating distance of blue light within the PCE increases and excites more converted yellow-green and red light. Furthermore, more blue light is absorbed by the lead frame owing to the stronger backward scattering effect of the nitride phosphor and the stronger total reflection effect between the PCE and the encapsulant. Moreover, the nitride phosphor with long-wavelength red light is also helpful in obtaining a lower CCT. Thus, the CCT generally decreases with increasing c_N. In addition, the lower CCT is less sensitive to the changes of the light mixing proportion in different viewing angles. The nitride phosphor also has a stronger ability to scatter the incident light. In particular, its SPD is more uniform than that of the YAG:Ce, which significantly contributes to the ACU. Therefore, the CCT distribution becomes more uniform with increasing c_N.

Fig. 10(a) shows the average CCT μ_{CCT} and the standard deviation CCT σ_{CCT} of the pcLED under three different c_{Y+N} values: 0.6 g/cm^3, 0.7 g/cm^3, and 0.8 g/cm^3. It is obvious that μ_{CCT} and σ_{CCT} decrease with the increasing c_{Y+N} mainly because of the increasing number of absorption and scattering events in the PCE. As explained in the discussion on CCT distribution above, μ_{CCT} and σ_{CCT} also decrease with the increasing c_N for a particular c_{Y+N}. Most interestingly, the PCE with lower c_{Y+N} and higher c_N can achieve a similar μ_{CCT} as that with higher c_{Y+N} and lower c_N. For instance, the μ_{CCT} near 8000 K can be obtained by $c_{Y+N} = 0.6$ g/cm^3 ($c_N = 40\%$) or $c_{Y+N} = 0.8$ g/cm^3 ($c_N = 30\%$) at the same time. However, their respective σ_{CCT} values differ greatly. The PCE with $c_{Y+N} = 0.8$ g/cm^3 ($c_N = 30\%$) can achieve a more uniform CCT distribution. In particular, σ_{CCT} decreases by 53.23% compared with that obtained by the PCE with $c_{Y+N} = 0.6$ g/cm^3 ($c_N = 40\%$). This means that the increasing

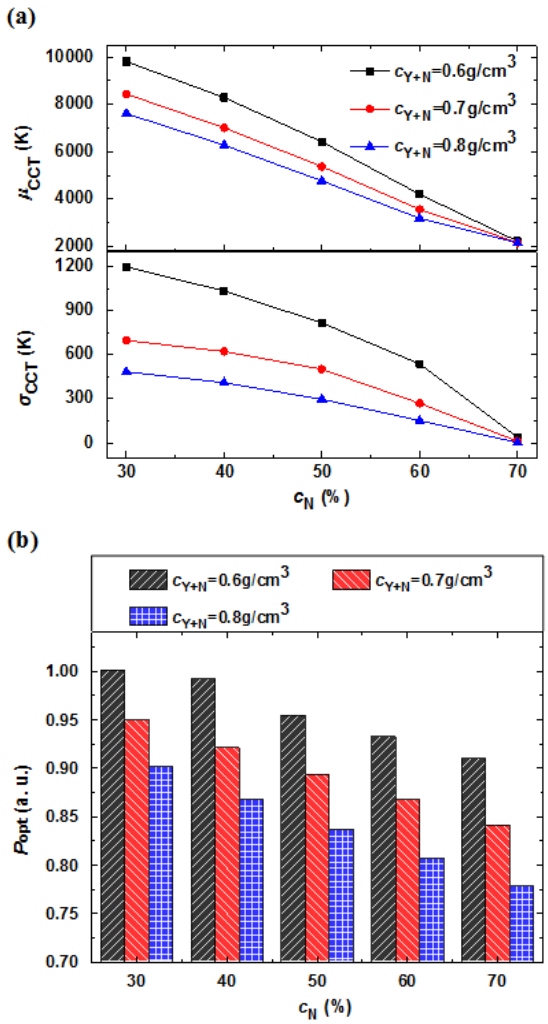

Fig. 10. (a) The average correlative color temperature (CCT) μ_{CCT}, the standard deviation CCT σ_{CCT}, and (b) the normalized light output power Popt of the phosphor-converted light-emitting diode (pcLED) with different total phosphor concentrations c_{Y+N} and nitride phosphor concentration c_N.

c_{Y+N} is the main factor in improving the ACU of pcLED for a given μ_{CCT}.

Fig. 10(b) shows the normalized P_{opt} of the pcLED. The P_{opt} decreases as c_{Y+N} increases owing to the larger amount of backward scattering and the color-conversion loss. Moreover, the increasing c_N can also lead to a decrease of the P_{opt} on account of the stronger backward scattering discussed above. However, it should be noted that the increasing c_{Y+N} is still the main factor in decreasing the P_{opt}. For instance, the P_{opt} obtained by $c_{Y+N} = 0.6$ g/cm^3 ($c_N = 40\%$) increases by 9.1% compared with that obtained by $c_{Y+N} = 0.8$ g/cm^3 ($c_N = 30\%$), these two types of configurations can both achieve the μ_{CCT} near 8000 K. This demonstrates that the PCE with lower c_{Y+N} and higher c_N can achieve a higher P_{opt} compared with the PCE with higher c_{Y+N} and lower c_N, at a similar μ_{CCT}.

V. Conclusion

In conclusion, by taking into account the irregular shapes of phosphors, the pcLED was successfully characterized by the FDTD method and simulated by the ray-tracing method. Our results show that the nitride phosphor more efficiently scatters the incident light to larger angles, though it also has much more backward scattering power, which is the result of its rod shape and high refractive index. We think that the phosphor particle shape has a significant effect on the scattering characterization, especially when the phosphor particle is oriented at different angles. Furthermore, the scattering and absorption parameters of phosphors were used to solve the optical properties of the PCE. Based on the common YAG:Ce and nitride phosphors with mean particle sizes of 13.7 μm and 5.2 μm, respectively, we have shown that increasing c_N can lead to an increase in μ_{sca}, μ_{abs}, and the refractive index, except for μ_{abs} (455 nm).

Finally, the optical performance of the pcLED containing the PCE above was investigated. We found that increasing c_{Y+N} and c_N can both lead to the improvement of the ACU and the loss of P_{opt}. The PCE with lower c_{Y+N} and higher c_N can achieve a higher P_{opt}, whereas the PCE with higher c_{Y+N} and lower c_N can achieve a more uniform CCT distribution for a similar μ_{CCT}. As a result, for applications demanding high P_{opt} values, the PCE with low c_{Y+N} and high c_N is recommended. However, for applications demanding high ACU, the PCE with high c_{Y+N} and low c_N is recommended. We think that the different scattering and absorption characterizations of the phosphors have a significant impact on the optical performance of the pcLED with multi-phosphor configuration. However, more studies on the PCE with multi-phosphor configuration are still necessary. The methodology introduced in this paper should provide detailed information for understanding the effect of phosphors (especially those with irregular shapes), and is important in discussing the optical performance of pcLEDs.

In the future, we plan to use this PCE characterization method to study the effect of the phosphor shape on the optical performance of pcLEDs. We believe that our findings will significantly contribute to the development of LED lighting applications.

References

[1] S. Pimputkar, J. S. Speck, S. P. DenBaars, and S. Nakamura, "Prospects for LED lighting," *Nature Photon.*, vol. 3, no. 4, pp. 180–182, 2009.

[2] C. Sommer *et al.*, "The effect of the phosphor particle sizes on the angular homogeneity of phosphor-converted high-power white LED light sources," *IEEE J. Sel. Topics Quantum Electron.*, vol. 15, no. 4, pp. 1181–1188, Jul./Aug. 2009.

[3] Y. Shuai, N. T. Tran, J. P. You, and F. G. Shi, "Phosphor size dependence of lumen efficiency and spatial CCT uniformity for typical white LED emitters," in *Proc. IEEE 62nd Electron. Compon. Technol. Conf. (ECTC)*, May/Jun. 2012, pp. 2025–2028.

[4] C. Sommer *et al.*, "The impact of light scattering on the radiant flux of phosphor-converted high power white light-emitting diodes," *J. Lightw. Technol.*, vol. 29, no. 15, pp. 2285–2291, Aug. 1, 2011.

[5] F. P. Wenzl *et al.*, "Impact of extinction coefficient of phosphor on thermal load of color conversion elements of phosphor converted LEDs," *J. Rare Earth.*, vol. 32, no. 3, pp. 201–206, 2014.

[6] R. Hu, Y. Wang, Y. Zou, X. Chen, S. Liu, and X. Luo, "Study on phosphor sedimentation effect in white light-emitting diode packages by modeling multi-layer phosphors with the modified Kubelka–Munk theory," *J. Appl. Phys.*, vol. 113, no. 6, p. 063108, 2013.

[7] C. Sommer *et al.*, "A detailed study on the requirements for angular homogeneity of phosphor converted high power white LED light sources," *Opt. Mater.*, vol. 31, no. 6, pp. 837–848, 2009.

[8] C. Sommer *et al.*, "Predicting solutions toward improved high power white LED light sources: A combined theoretical and experimental study," *Proc. SPIE*, vol. 7103, p. 710309, Sep. 2008.

[9] C. Sommer *et al.*, "The impact of inhomogeneities in the phosphor distribution on the device performance of phosphor-converted high-power white LED light sources," *J. Lightw. Technol.*, vol. 28, no. 22, pp. 3226–3232, Nov. 15, 2010.

[10] Z.-Y. Liu, S. Liu, K. Wang, and X.-B. Luo, "Studies on optical consistency of white LEDs affected by phosphor thickness and concentration using optical simulation," *IEEE Trans. Compon. Packag. Technol.*, vol. 33, no. 4, pp. 680–687, Dec. 2010.

[11] Z. Liu, S. Liu, K. Wang, and X. Luo, "Optical analysis of phosphor's location for high-power light-emitting diodes," *IEEE Trans. Device Mater. Rel.*, vol. 9, no. 1, pp. 65–73, Mar. 2009.

[12] R. Yu, S. Jin, S. Cen, and P. Liang, "Effect of the phosphor geometry on the luminous flux of phosphor-converted light-emitting diodes," *IEEE Photon. Technol. Lett.*, vol. 22, no. 23, pp. 1765–1767, Dec. 1, 2010.

[13] H. Zheng, X. Fu, B. Wu, S. Liu, and X. Luo, "A method for geometry control of phosphor layer in high-power white LEDs by package structure," in *Proc. 14th Int. Conf. Electron. Mater. Packag. (EMAP)*, 2012, pp. 1–5.

[14] H. Zheng, X. Fu, R. Hu, S. Liu, and X. Luo, "Angular color uniformity improvement for phosphor-converted white light-emitting diodes by optimizing remote coating phosphor geometry," in *Proc. 13th Int. Conf. Electron. Packag. Technol. High Density Packag. (ICEPT-HDP)*, Aug. 2012, pp. 1483–1486.

[15] K.-J. Chen *et al.*, "Enhanced luminous efficiency of WLEDs using a dual-layer structure of the remote phosphor package," *J. Lightw. Technol.*, vol. 31, no. 12, pp. 1941–1945, Jun. 15, 2013.

[16] Z.-Y. Liu, C. Li, B.-H. Yu, Y.-H. Wang, and H.-B. Niu, "Uniform white emission of WLEDs realized by multilayer phosphor with pyramidal shape and inversed concentration distribution," *IEEE Photon. Technol. Lett.*, vol. 24, no. 17, pp. 1558–1560, Sep. 1, 2012.

[17] Y. Zhou, J. Lin, M. Yu, S. M. Han, S. B. Wang, and H. J. Zhang, "Morphology control and luminescence properties of YAG:Eu phosphors prepared by spray pyrolysis," *Mater. Res. Bull.*, vol. 38, no. 8, pp. 1289–1299, 2003.

[18] W. Q. Chen, D. S. Jo, Y. H. Song, T. Masaki, and D. H. Yoon, "Synthesis and photoluminescence properties of YAG:Ce^{3+} phosphor using a liquid-phase precursor method," *J. Lumin.*, vol. 147, pp. 304–309, Mar. 2014.

[19] Z. Liu, S. Liu, K. Wang, and X. Luo, "Status and prospects for phosphor-based white LED packaging," *Frontiers Optoelectron. China*, vol. 2, no. 2, pp. 119–140, 2009.

[20] M. Yamada *et al.*, "Red-enhanced white-light-emitting diode using a new red phosphor," *Jpn. J. Appl. Phys.*, vol. 42, no. 1A, p. L20, 2003.

[21] L. Chen, C.-I. Chu, and R.-S. Liu, "Improvement of emission efficiency and color rendering of high-power LED by controlling size of phosphor particles and utilization of different phosphors," *Microelectron. Rel.*, vol. 52, no. 5, pp. 900–904, 2012.

[22] J. P. You, N. T. Tran, and F. G. Shi, "Light extraction enhanced white light-emitting diodes with multi-layered phosphor configuration," *Opt. Exp.*, vol. 18, no. 5, pp. 5055–5060, 2010.

[23] Z.-T. Li, Y. Tang, Z.-Y. Liu, Y.-E. Tan, and B.-M. Zhu, "Detailed study on pulse-sprayed conformal phosphor configurations for LEDs," *J. Display Technol.*, vol. 9, no. 6, pp. 433–440, 2013.

[24] C.-W. Sher *et al.*, "Enhancement of luminous efficiency by hybrid structure for warm white light-emitting diodes," *J. Solid State Lighting*, vol. 1, p. 9, Jul. 2014.

[25] S. T. Flock, M. S. Patterson, B. C. Wilson, and D. R. Wyman, "Monte Carlo modeling of light propagation in highly scattering tissues. I. Model predictions and comparison with diffusion theory," *IEEE Trans. Biomed. Eng.*, vol. 36, no. 12, pp. 1162–1168, Dec. 1989.

[26] W. J. Wiscombe, "Improved Mie scattering algorithms," *Appl. Opt.*, vol. 19, no. 9, pp. 1505–1509, 1980.

[27] P. Yang, K. N. Liou, M. I. Mishchenko, and B.-C. Gao, "Efficient finite-difference time-domain scheme for light scattering by dielectric particles: Application to aerosols," *Appl. Opt.*, vol. 39, no. 21, pp. 3727–3737, 2000.

[28] M. I. Mishchenko, L. D. Travis, R. A. Kahn, and R. A. West, "Modeling phase functions for dustlike tropospheric aerosols using a shape mixture of randomly oriented polydisperse spheroids," *J. Geophys. Res. Atmos.*, vol. 102, pp. 16831–16847, Jul. 1997.

[29] S.-L. Hsiao, N.-C. Hu, and H. Cornelissen, "Phosphor-converted LED modeling using near-field chromatic luminance data," *Opt. Exp.*, vol. 21, no. 52, pp. A250–A261, 2013.

[30] C.-H. Hung and C.-H. Tien, "Phosphor-converted LED modeling by bidirectional photometric data," *Opt. Exp.*, vol. 18, no. S3, pp. A261–A271, 2010.

[31] K.-J. Chen *et al.*, "An investigation of the optical analysis in white light-emitting diodes with conformal and remote phosphor structure," *J. Display Technol.*, vol. 9, no. 11, pp. 915–920, Nov. 2013.

[32] K. Yee, "Numerical solution of initial boundary value problems involving Maxwell's equations in isotropic media," *IEEE Trans. Antennas Propag.*, vol. 14, no. 3, pp. 302–307, May 1966.

[33] A. R. Jones, "Light scattering for particle characterization," *Prog. Energ. Combustion Sci.*, vol. 25, no. 1, pp. 1–53, 1999.

[34] Z. Liu, S. Liu, K. Wang, and X. Luo, "Measurement and numerical studies of optical properties of YAG:Ce phosphor for white light-emitting diode packaging," *Appl. Opt.*, vol. 49, no. 2, pp. 247–257, 2010.

[35] L. O. Reynolds and N. J. McCormick, "Approximate two-parameter phase function for light scattering," *J. Opt. Soc. Amer.*, vol. 70, no. 10, pp. 1206–1212, 1980.

[36] X. Ding, J. Li, Q. Chen, Y. Tang, Z. Li, and B. Yu, "Improving LED CCT uniformity using micropatterned films optimized by combining ray tracing and FDTD methods," *Opt. Exp.*, vol. 23, no. 3, pp. A180–A191, 2015.

Jia-Sheng Li received the B.E. degree in mechanical engineering and automation from the South China University of Technology, Guangzhou, China, in 2014.

He is currently pursuing the master's degree with the Key Laboratory of Surface Functional Structure Manufacturing of Guangdong, Higher Education Institutes, South China University of Technology. His current research focuses on the LED packaging and lighting quality.

Jia-Xiao Chen received the B.E. degree in mechanical engineering and automation from the South China University of Technology, Guangzhou, China, in 2014.

He is currently pursuing the master's degree with the Key Laboratory of Surface Functional Structure Manufacturing of Guangdong, Higher Education Institutes, South China University of Technology. His current research focuses on the LED packaging process and reliability.

Li-Wei Lin received the B.S. degree in power mechanical engineering from the National Tsing Hua University, Taiwan, in 1986, and the M.S. and Ph.D. degrees in mechanical engineering from the University of California, Berkeley, in 1991 and 1993, respectively.

He currently serves as the Chancellor's Professor of the Department of Mechanical Engineering with the University of California, Berkeley, and the Co-Director of the Berkeley Sensor and Actuator Center. His research interests and activities include microelectromechanical systems, nanoelectromechanical systems, nanotechnology, and microelectronics.

Zong-Tao Li received the Ph.D. degree in mechanical engineering with a minor in microelectronics manufacture engineering from the South China University of Technology, Guangzhou, China, in 2014.

He is currently with the Key Laboratory of Surface Functional Structure Manufacturing of Guangdong, Higher Education Institutes, South China University of Technology, and the Optoelectronics Engineering Technology Research and Development Center, Foshan NationStar Optoelectronics Company, Ltd., Foshan, China. His major research interests include packaging of high-power LEDs, lighting quality, and device reliability.

Yong Tang received the Ph.D. degree in mechanical engineering from the South China University of Technology, Guangzhou, China, in 1994. He has over ten years of experience in surface coating technology and over eight years in optoelectronic LED packaging.

He is currently a Professor with the School of Mechanical and Automotive Engineering, South China University of Technology, and the Director of the Key Laboratory of Surface Functional Structure Manufacturing of Guangdong, Higher Education Institutes, Guangdong. His research interests include surface properties in clean energy and its high efficient usage, especially in energy-saving solid-state lighting.

Bin-Hai Yu received the Ph.D. degree in mechanical and electronic engineering from the Huazhong University of Science and Technology, Wuhan, China, in 1997.

He joined Foshan Nationstar Optoelectronics Company, Ltd., Foshan, China. He was a Post-Doctoral Researcher with Foshan Enterprise Post-Doctoral Work Station from 1999 to 2001. He became the Vice Chairman from 2007 to 2014. He is currently a Professor with the School of Mechanical and Automotive Engineering, South China University of Technology, Guangzhou, China, and the Key Laboratory of Surface Functional Structure Manufacturing of Guangdong, Higher Education Institutes, Guangdong. His research includes the LED luminaire, SMD LED, high-power LED packaging, and new packaging process.

Xin-Rui Ding received the Ph.D. degree in mechanical engineering with a minor in microelectronics manufacture engineering from the South China University of Technology, Guangzhou, China, in 2015.

He is currently with the Key Laboratory of Surface Functional Structure Manufacturing of Guangdong, Higher Education Institutes, South China University of Technology. His major research interests include the LED packaging, lighting quality, and reliability.

View publication stats